Macromolecules

ARTICLE

pubs.acs.org/Macromolecules

Multiple Morphologies of PAA-*b*-PSt Assemblies throughout RAFT Dispersion Polymerization of Styrene with PAA Macro-CTA

Wei-Dong He,* Xiao-Li Sun, Wen-Ming Wan, and Cai-Yuan Pan

Department of Polymer Science and Engineering, CAS Key Laboratory of Soft Matter Chemistry, University of Science and Technology of China, Hefei, Anhui, 230026, China

Supporting Information

ABSTRACT: The assembly behavior of diblock copolymers in solution can be modulated by block length, block ratio, solvent properties, and preparation route. Different assembly morphologies such as spherical micelles, cylindrical micelles, vesicles, and large compound vesicles have been obtained for diblock copolymers with shorter solvated block, such as poly(acrylic acid)-*b*-polystyrene (PAA-*b*-PSt). In the present work, we reported an easy-going route to prepare PAA-*b*-PSt assemblies with different morphologies through reversible addition−fragmentation-transfer (RAFT) dispersion polymerization of styrene in methanol with trithiocarbonated PAA as macromolecular chain transfer agent. Because this RAFT dispersion polymerization exhibited controlled features, the consecutive growth of PSt block led to the successive transition of the obtained PAA-*b*-PSt assemblies from spherical micelles, cylindrical micelles, vesicles, to large compound vesicles, confirmed by the combination of electron microscopy, laser light scattering, and chemical structural analysis. PAA-*b*-PSt assembly morphologies and their transition have been adjusted by polymerization conversion, St/PAA feed ratio, and methanol amount, which were elucidated in view of thermodynamic consideration. The mechanisms for the formation of vesicle and the reorganization of vesicles were suggested. This polymerization-induced self-assembly and self-organization provides an efficient way to prepare different nano/microsized polymeric structures.

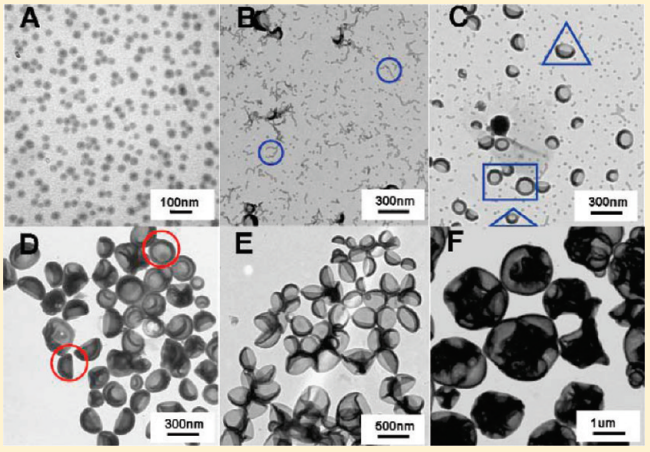

INTRODUCTION

Polymeric assemblies in solutions, which hold comprehensive structures and controlled dimensions, have gained increasing research interest, especially because of a series of reports about poly(acrylic acid)-*b*-polystyrene (PAA-*b*-PSt) assemblies in selective solvents from Eisenberg's group.[1−4] Many efforts have also been presented by others to modulate the assembly morphology,[5−7] elucidate the thermodynamics and mechanism,[8−11] and investigate kinetically the formation of assemblies.[12−15] Meanwhile, the potential applications of block copolymer assemblies are focused mainly on biomedical areas, such as drug carriers, gene delivery, biodiagnosis, and bioimaging.[16−21]

Polymer assemblies in solution commonly include spherical micelles, cylindrical micelles, vesicles, and large compound vesicles. Other polymer assemblies with exceptional shapes are also reported. Some of them have been identified, such as knedel-like structure,[22] spaghetti structure,[23] Janus micelles,[24] and kippah vesicle.[25] Lamellar micelles, which were supposed as an intermediated morphology between cylindrical micelles and vesicles, were reported to occasionally be observed by Eisenberg's group.[2] Those artificial polymer assemblies bear the resemblance to cell organizations as well as the assemblies from small molecular surfactants.

Most of polymer assemblies in solution are built up through the self-assembly of amphiphilic copolymers in selective solvents. Those copolymers can be block copolymers,[26−28] which are the most studied, graft copolymers,[29,30] segmented copolymers with versatile architectures,[31−33] and even random copolymers.[34,35] The pioneering researches were mainly paid to the micelles, with symmetrical insight into the influences of preparation parameters and scaling dependences of micelle structure on block lengths.[36−40] Now, the dependences of block copolymer assemblies on copolymer chemical structure and solvent variation have been illuminated, and many novel assembled structures have been disclosed. However, this strategy is involved in multistage preparation, including at least the preparation of amphiphilic copolymers and their self-assembly in selective solvents. Meanwhile, diluted solution and precautious preparation make the scale-up production and reproductivity of the aimed morphologies difficult.

Therefore, considerable efforts have been expended on the facile fabrication of multiple morphologies of copolymer assemblies.

Received: January 12, 2011
Revised: March 31, 2011
Published: April 11, 2011

Wu et al. first proposed the chemistry-induced self-assembly of block copolymer to obtain polystyrene-*b*-polyacetylene from the elimination of polystyrene-*b*-poly(vinyl phenyl sulfoxide).[41] Chen et al. prepared the micelle dispersion of polystyrene-*b*-poly (vinyl pyridine) with the concentration up to 200 g/L through the cross-linkage of poly(vinyl pyridine) with 1,4-dibromobutane.[42,43] On the basis of the strategy of chemistry-induced self-assembly, we developed a polymerization-induced self-assembly method to obtain various nanostructured particles.[44−47] In this strategy, solvated macroinitiators for living radical polymerizations, such as atom transfer radical polymerization (ATRP) and reversible addition−fragmentation-transfer (RAFT) polymerization, are adopted, and the polymerizations are carried out in selective solvents. In the living radical dispersion polymerizations, the successive increase in insoluble block leads to the formation and transition of different assemblies. For example, dispersion ATRP of 4-vinyl pyridine (4-VP) in ethanol/water mixture with 2-bromoisobutyrylated poly(ethylene glycol) (PEG) resulted in only spherical micelles,[48] and RAFT dispersion polymerization of styrene (St) in methanol with *S*-1-dodecyl-*S*-(a,a'-dimethyl-α''-acetic acid)-trithiocarbonate (TTC)-terminated P4VP yielded spherical micelles, vesicles, and nanowires of P4VP-*b*-PSt assemblies.[44−47]

Actually, living/controlled radical emulsion and dispersion polymerizations have been widely investigated. Under appropriate circumstances, living features were observed in view of the linear dependence of molecular weight on conversion, narrow molecular weight distribution, and the ability of block copolymerization.[49−54] Some of the living/controlled radical emulsion and dispersion polymerizations afford spherical particles with uniform size.[53−55] Few of them involving in macroinitiators or macro chain transfer agent (CTA) produced polymer particles with distinctive morphologies. Charleux et al. utilized TTC-terminated PEG (M_n = 2000) as macro-CTA to carry out surfactant-free emulsion polymerizations of *n*-butyl acrylate and methyl methacrylate and observed raspberry-like particles with inner water-pools.[49] With TTC-terminated random copolymer of acrylic acid and PEG acrylate, Charleux et al. also obtained nanofibers via RAFT polymerization of styrene in water.[56] Just recently, Li and Armes performed RAFT aqueous dispersion polymerization of 2-hydroxypropyl methacrylate (HPMA) with poly(glycerol monomethacrylate) macro-CTA as the reactive steric stabilizer.[57] Varying the length of PHPMA block chains allowed the precise modulation of final size (20−100 nm) of the nanoparticles. Moreover, longer core-forming PHPMA blocks led to the in situ formation of vesicles with the diameter of ∼500 nm.

In this manuscript, we further extended polymerization-induced self-assembly to RAFT dispersion polymerization of St with PAA macro-CTA in methanol. Throughout the polymerization, the morphology transition from spherical micelles, cylindrical micelles, and vesicles, to large compound vesicles (LCVs) was observed with the continuous increase in PSt block. This strategy offers an easy and scaled-up way to prepare multiple self-assembly structures.

EXPERIMENTAL SECTION

Materials. Styrene (St, Shanghai Chem., >99%) was washed with an aqueous solution of sodium hydroxide (5 wt %) three times and then washed with water. After being dried with anhydrous magnesium sulfate, St was distilled under reduced pressure before use. Acrylic acid (AA, Shanghai Chem., 96%) was dried over anhydrous magnesium sulfate and then distilled under reduced pressure prior to use. 2,2′-Azobisisobutyronitrile (AIBN) was purified by recrystallization from ethanol. Tetrahydrofuran (THF) was distilled over sodium/benzophenone prior to use. 2-Dodecylsulfanyl- thiocarbonylsulfanyl-2-methylpropinoic acid (DMP, i.e., TTC) was synthesized as previously described.[58] Other reagents with analytical grade were used as received.

Preparation of DMP-Terminated Poly(acrylic acid) (PAA-DMP). Author: AA (7.20 g, 0.1 mol), DMP (364 mg, 1 mmol), THF (8.0 mL), and AIBN (16.4 mg, 0.1 mmol) with the molar ratio of AA/DMP/AIBN 1000:10:1 were added to a 25 mL polymerization vial with a magnetic bar. After three freeze−evacuate−thaw cycles, the vial was sealed under high vacuum and placed in an oil bath at 80 °C while stirring. After 2 h, the vial was cooled to room temperature with ice−water and opened. PAA-DMP (3.97 g) was obtained by the precipitation of polymerization mixture into excess diethyl ether under filtration and vacuum dryness at room temperature overnight. The conversion measured by proton nuclear magnetic resonance (^{1}H NMR) method was 61%. The number-averaged block length of PAA block by ^{1}H NMR analysis (L_{PAA}) was determined to be 61. ^{1}H NMR, DMSO-d_6, δ (TMS): 0.86 (m, 3H, −C$\underline{H}_3$), 1.15−2.34 (m, −C$\underline{H}_2$C$\underline{H}$−), 3.32 (t, 2H, −C$\underline{H}_2$S), 12.21(s, 1H, −COO$\underline{H}$). Molecular weight polydispersity (M_w/M_n) was determined to be 1.13 by gel permeation chromatograph (GPC).

RAFT Dispersion Polymerization of St with PAA-DMP. PAA-DMP, St, AIBN, and methanol with certain amounts were added to a 5 mL glass vial equipped with a magnetic bar. After clear solution was obtained, the mixture was degassed by three freeze−pump−thaw cycles. The vial was sealed under vacuum and placed in an oil bath of 80 °C with stirring. After polymerization was carried out for the prescribed time, the reaction mixture was cooled to room temperature with ice−water, and the vial was opened. A weighted portion of the obtained dispersion was taken out for the morphology observation by electron microscopies and the study of laser light scattering (LLS). Then, polymer was obtained by the precipitation into excess petroleum ether, purification by the reprecipitation, and dryness under vacuum. The conversion of St was determined gravimetrically. ^{1}H NMR spectroscopy was used to determine the block length of PSt (L_{PSt}).

Characterization. NMR spectra were measured on a Bruker DMX300 NMR spectrometer in DMSO-d_6 or pyridine-d_5 using tetramethylsilane as an internal reference. Relative number-average molecular weight (M_{nGPC}) and molecular weight distribution of PAA were measured on a Waters 515 GPC instrument equipped with Ultrahydrogel 250 and 500 columns using PEO as the calibration standard. An aqueous solution of Na_2HPO_4−NaH_2PO_4 (pH 7.0, 0.2 M) was used as the eluent at a flow rate of 1.0 mL/min. For GPC characterization of PAA-*b*-PSt, the copolymers were first converted to poly(methyl acrylate)-*b*-PSt with trimethylsilyldiazomethane,[59] and GPC performance was conducted on Waters 150C GPC equipped with three Ultrastyragel columns (500, 10^3, 10^4 Å) in series and refractory index detector (RI 2414) at 30 °C using monodispersed polystyrene as calibration standard. THF was used as eluent at a flow rate of 1.0 mL/min.

Transmission electron microscope (TEM) observation was carried out on a Hitachi H-800 TEM instrument at an accelerating voltage of 200 kV. One drop of the thinned polymerization mixture in methanol was deposited on copper grids. The solvent and the residual monomers were evaporated at room temperature for 2−3 d. TEM samples obtained were not stained. A field emission scanning electron microscope (FESEM) observation was performed on a JEOL 6700F. FESEM samples were prepared similarly and gilded before the observation. LLS studies were conducted with a modified commercial LLS spectrometer (ALV/SP-125) equipped with an ALV-5000 multi-τ digital time correlator and a solid-state laser (ADLAS DPY42511, out power was ∼400 mW at λ = 532 nm). Dynamic light scattering was performed at

Scheme 1. Synthesis of PAA-*b*-PSt through RAFT

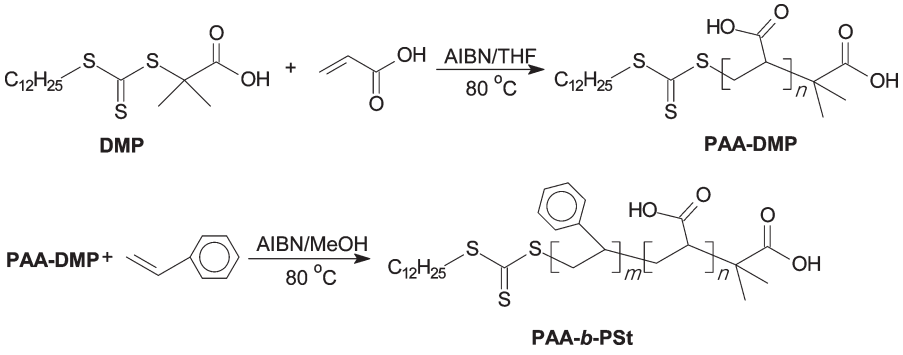

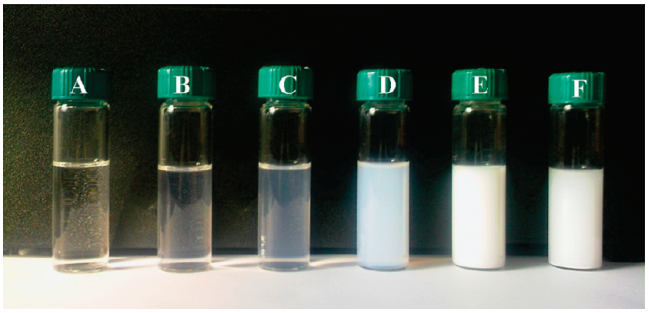

Figure 1. Digital photos of polymerization mixtures at different polymerization time: (A) 0, (B) 1, (C) 3.5, (D) 6, (E) 9, and (F) 16 h.

25 °C and a fixed scattering angle of 30°. The data were processed with both Cumulants and CONTIN calculation. Static light scattering (SLS) studies were conducted at 25 °C using the same instrument at scattering angles ranging from 30 to 150°. The radius of gyration (R_g) data were obtained using standard *Zimm* plot analysis.

RESULTS AND DISCUSSION

In this article, DMP-terminated poly(acrylic acid) with L_{PAA} of 61 was obtained via RAFT polymerization of AA in THF. RAFT dispersion polymerizations of St were performed in methanol using PAA-DMP as both macro-CTA and stabilizer. The polymer synthesis is shown in Scheme 1. Methanol was chosen as the polymerization medium because it is a good solvent of St and PAA but a nonsolvent of PSt. Before the polymerization occurred, the mixture was homogeneous and clear, as shown in Figure 1A. In the initial polymerization, the growing PAA-*b*-PSt copolymer remained soluble in the reaction mixture because the PSt block was still relatively short. When the length of PSt block increased to past a critical value, microphase separation took place to induce the formation of spherical micelles with PSt core and PAA corona through PAA-*b*-PSt assembly. Therefore, the polymerization mixture turn bluish at 1 h (Figure 1B). With the polymerization further proceeding, the mixture turn translucent, opaque, and then completely white. This observation suggests the increase in both size and number of the formed assemblies.

Living Features for RAFT Dispersion Polymerization of St. To understand the mechanism of phase separation and morphology transition in polymerization-induced assembly, we confirmed living features of RAFT dispersion polymerization. (The details appear in the Supporting Information.)

The first-order kinetics to monomer and linear dependence of molecular weight on conversion was roughly observed in the range of monomer conversion between 15 and 63%. GPC result demonstrates the increase in molecular weight with polymerization time and narrow distribution of molecular weight. The living/control features of the current RAFT dispersion polymerizations would make it possible for PAA-*b*-PSt assemblies to undertake in situ successive morphology transition. The composition of PAA-*b*-PSt at different polymerization time is illustrated in Table 1.

Successive Morphology Transition of PAA-*b*-PSt during RAFT Dispersion Polymerization. Eisenberg et al. have explored the morphology transition of PAA_x-*b*-PSt_y (x and y denote the polymerization degree of PAA and PSt block, respectively) with the change of solvent selectivity,[4,60] such as the composition of solvent mixture, pH, and salt concentration. They also investigated the influences of block length and block ratio on the formed morphology.[61,62] Their comprehensive investigation of the postpolymerization assembly offers the excellent comparison with our polymerization-induced assembly of PAA-*b*-PSt, where PSt block length is continuously increased during RAFT dispersion polymerization while PAA block length keeps unchanged.

Figure 2 offers an example of successive transition of PAA-*b*-PSt during RAFT dispersion polymerization of St with PAA-DMP macro-CTA. At the beginning of polymerization, PAA_{61}-CTA was totally dissolved in the polymerization mixture, and the system was clear (Figure 1A). Within a short duration <1 h, the polymerization mixture remained transparent because L_{PSt} of the resulted PAA-*b*-PSt was still low. At 1 h of polymerization time, L_{PSt} reached 132 and exceeded the first critical value to induce the association of PSt blocks. Thus, spherical micelles with PSt as the core and PAA as the shell were formed. The micelles were much smaller, observed from TEM images and DLS characterization (Figure 3). At 2 h, L_{PSt} was 189, and the micelles kept the spherical shape with a little increase in their size.

The formation of block copolymer assemblies in a selective solvent is primarily dependent on thermodynamic permission; in other words, the change of free energy (ΔG) should be negative for certain processes.[63] As for the formation of spherical micelles, the negative value of enthalpy change (ΔH) is favorable mainly because of the stronger affinity interaction among PSt blocks than that between PSt blocks and medium molecules. Favorable enthalpy change may also be attributed to the corona-forming blocks of PAA because of the increase in the medium polarity with monomer consumption. On the basis of the conformation

Table 1. Characteristics of Various Morphologies Formed during RAFT Dispersion Polymerization[a]

time (h)	PAA-*b*-PSt	morphology	D[b]	R_h (nm)[c]
1	PAA_{61}-*b*-PSt_{132}	spherical micelles	26 nm	14
2	PAA_{61}-*b*-PSt_{189}	spherical/cylinderical micelle	32 nm	19
3.5	PAA_{61}-*b*-PSt_{251}	spherical/cylinderical micelle	32 nm	20
		vesicle	205 nm	109
6	PAA_{61}-*b*-PSt_{347}	spherical/cylinderical micelle	41 nm	21
		vesicle	237 nm	119
9	PAA_{61}-*b*-PSt_{452}	vesicle	280 nm	155
16	PAA_{61}-*b*-PSt_{596}	adjoining vesicle	300 nm∼1 μm	168
				787
20	PAA_{61}-*b*-PSt_{655}	large compound vesicle	300 nm∼1 μm	477
24	PAA_{61}-*b*-PSt_{704}	large compound vesicle	1 μm	428

[a] Polymerization condition: PAA-DMP/St/AIBN 10:10000:1 (in moles); St = 1.04 g; methanol = 1.00 g; 80 °C. [b] Measured by TEM. [c] Measured by LLS.

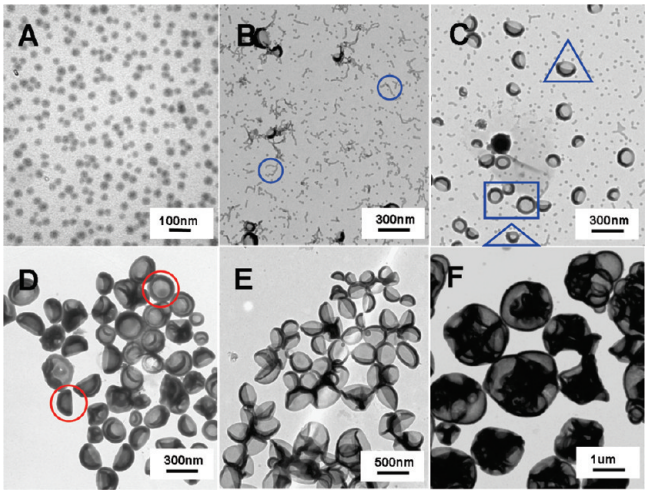

Figure 2. TEM images of PAA-*b*-PSt assemblies formed at different polymerization time: (A) 1, (B) 3.5, (C) 6, (D) 9, (E) 16, and (F) 24 h. PAA-DMP/St/AIBN 10:10000:1 (in mole); St = 1.04 g; methanol = 1.00 g; 80 °C.

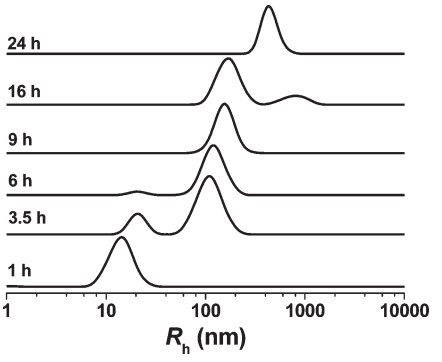

Figure 3. R_h distribution of PAA-*b*-PSt assemblies at different time of RAFT dispersion polymerization.

change of both PSt and PAA blocks, the contribution of entropy is unfavorable to the formation of micelles for PSt-*b*-PAA chains. However, the change of the solvent composition might bring out the negative value of entropy change (ΔS). In all, the formation of micelles for PSt-*b*-PAA chains in the medium is spontaneous.

As mentioned by Eisenberg et al.,[64] the formation of crew-cut micellar aggregates is controlled by the stretching degree of PSt core-forming block (entropy concern), the repelling interaction of PAA corona-forming block (both entropy and enthalpy concerns), and core−corona interfacial energy (enthalpy concern). In the present case, the block length of PAA (L_{PAA}) was constant, and the enthalpy contribution from PAA blocks could be regarded as unchanged throughout the polymerization. The core−corona interfacial energy is the product of interfacial tension and interfacial area, where the former is constant and the latter has the tendency to keep the minimum value. With the increase in L_{PSt}, PSt blocks have to stretch to greater extent, especially in the core region adjacent to the interface, resulting in the protuberance of core-forming PSt blocks into the surrounding medium.[65] Therefore, spherical micelles of PAA_{61}-*b*-PSt_{251} would deform the shape and fuse with each other at 3.5 h, and the transition of spherical micelles to cylindrical micelles occurred. At this moment, L_{PSt} was above the second critical value for the transition of assembly morphology. The fusion process of several spherical micelles into cylindrical morphology is distinguished with blue circles in Figure 2B. The most sighted morphology at this moment is cylindrical micelle with the same diameter as spherical micelle and the length of 100−300 nm. That is to say, cylindrical micelles have a relatively narrow diameter distribution but a widely variable length.

At 6 h (L_{PSt} = 347), cylindrical micelles were seldom found, and vesicle morphology was mainly sighted, as shown in Figure 2C. Upon the formation of many vesicles with large size, the polymerization mixture became more opaque. The vesicles had different perfection and diameter. However, their wall thickness was almost the same (30 nm). As they did in spherical micelles, PSt chains in cylindrical micelles also underwent different stretching degree, relying on their length and location relative to the interface. Thus, as L_{PSt} exceeded the third critical value, the shape of cylindrical micelles should transform and the next transition of assembles morphology would happen. Although lamellar micelles were suggested to be the intermorphology between cylindrical micelles and vesicles,[2] they were not observed by us.

The coexistence of multiple morphologies can be obviously observed in Figure 2B,C. This phenomenon might be caused by the polydispersity of copolymer composition and the

dx.doi.org/10.1021/ma2000674 |*Macromolecules* 2011, 44, 3358–3365

Table 2. Characteristics of Morphologies for RAFT Dispersion Polymerization at Different St/PAA-DMP[a]

PAA-*b*-PSt	St/PAA-DMP	Conv	morphologies	D^b	R_h (nm)[c]
PAA_{61}-*b*-PSt_{198}	250	79.2	spherical/cylinderical micelle	29 nm	20
PAA_{61}-*b*-PSt_{379}	500	75.8	vesicle	185 nm	101
PAA_{61}-*b*-PSt_{537}	750	71.6	aggregated vesicle	200 nm∼1.5 μm	552
PAA_{61}-*b*-PSt_{704}	1000	70.4	compound vesicle	500 nm∼1 μm	447
PAA_{61}-*b*-PSt_{842}	1250	67.3	compound vesicle	1.4 μm	733

[a] Polymerization condition: PAA-DMP/AIBN 10:1 (in mole); St = 1.04 g; methanol = 1.00 g; 80 °C, 20 h. [b] Measured by TEM. [c] Measured by LLS.

crossover of stability boundaries for various morphologies.[64] For an example, spherical micelles with longer corona PAA chains can hold longer core PSt chains, and the second critical L_{PSt} for the morphology transition from spherical micelle to cylindrical micelle should have a larger value.

It is worthily noted that few hemispherical vesicles (named as kippah vesicle) were visible at 3.5 h, and the vesicles with relative full circle have not been observed until the polymerization time of 6 h. Azzam and Eisenberg contributed the formation of kippah vesicles to the indentation of common vesicles, caused by the negative osmotic pressure from the diffusion difference of water and dioxane.[25] However, the current observation suggests that kippah vesicles would grow perfect by absorbing free micelles onto their open periphery, as evidenced in Figure 2C (blue triangle).

As the polymerization proceeded to 9.0 h, L_{PSt} reached 452. Spherical and cylindrical micelles became thermodynamically unstable and emerged into the vesicles. Thus, the micelles completely disappeared and the vesicles varied obviously in their size and morphology. Some of the vesicles have double walls, and the inner is commonly open. We presume that these double-walled vesicles were formed through the endouptaking of small vesicle by large vesicle. Meanwhile, the walls of different vesicles might have the possibility of merging with each other to result in the increase in wall thickness, as illustrated with red circles in Figure 2D. At this moment, most vesicles existed separately while few vesicles combined with each other through wall fusion. The transition from simple vesicle to large compound vesicle can be ensued through two mechanisms. Endo-uptaking needs the open structure of larger vesicles and occurs in the initial stage of this transition. Wall fusion results from the increase in stretching degree of PSt chains and happens throughout this transition. Because styrene likely stayed in the PSt-enriched region of vesicle wall, PSt chain rearrangement and PSt wall fusion might be possible.

Because the polymerization exhibited living features, the further prolongation of polymerization increased PSt block length and prompted the incorporation and growth of vesicles. As shown in Figure 2E (16 h), almost all vesicles adjoined by their walls to form large vesicle aggregates, where few small wrinkled vesicles were interconnected. With more and more vesicles combined, large compound vesicles with alveolus pulmonis-like structure were observed at the polymerization of 24 h. The average diameter of LCVs ranges from 1 to 2 μm.

The morphology variation during RAFT dispersion polymerization was also followed by dynamic light scattering and SLS. Figure 3 shows the hydrodynamic radius (R_h) distribution of copolymer assemblies at different polymerization time. Combined with TEM observation, we could deduce the following observation. At 1 h, only one peak at R_h = 14 nm was observed, and the ratio of gyration radius to R_h was determined to be 0.78, indicating that PAA_{61}-*b*-PSt_{189} assemblies were solid spherical micelles. At 2 h, R_h was 19 nm, and the micelles gradually lost the spherical shape. At 3.5 h, hydrodynamic radius distribution turned bimodal. The peak at higher R_h (109 nm) should be attributed to spherical vesicles and that at lower R_h (20 nm) should be attributed to micelles. At 6 h, hydrodynamic radius distribution was still bimodal (peak values of R_h = 21 and 119 nm) whereas the ratio of peak area obviously changed, indicating that more and more micelles converted to vesicles. The transition of the micelle to the vesicle was completed at 9 h, and unimodal hydrodynamic radius distribution was observed again with the increase in R_h to 155 nm. At 16 h, the simple vesicles had started to combine each other through the wall fusion, and bimodal hydrodynamic radius distribution was detected again. The peak with larger R_h (780 nm) should be ascribed to the large compound vesicles undertaking the wall fusion. The peak with lower R_h moved to 168 nm, suggesting the increase in vesicle size and/or wall thickness. With the prolongation to 20 h, large compound vesicles were formed and behaved as a unity, and thus unimodal hydrodynamic radius distribution came back once more and R_h became 477 nm. Further increasing the polymerization time to 24 h, LCVs with more compact structure were produced and R_h fell to 428 nm, which might caused by the rearrangement of PSt chains and PSt-rich regions.

Influence of St/PAA-DMP Molar Ratio on Assembly Morphology. L_{PSt} can also be modulated with the molar ratio of St to PAA-DMP. Thus, RAFT dispersion polymerizations of St (1.04 g, 10 mmol) in methanol (1.00 g) were performed with different amounts of PAA-DMP at 80 °C for 20 h. The ratio of PAA-DMP to AIBN was kept at 10, and the molar ratio of St to PAA-DMP varied at 250, 500, 750, 1000, and 1250. The results are summarized in Table 2. TEM and SEM images are shown in Figures 4 and 5, respectively.

When the molar ratio of St/PAA-DMP was 250, the spherical and cylindrical micelles of PAA_{61}-*b*-PSt_{189} coexisted. The diameters of both cylindrical micelle and spherical micelle were approximately the same (29 nm), evidenced in Figure 4A. SEM images of Figure 5A,B also demonstrate the curvy contour of some cylindrical micelles, suggesting that the cylindrical micelles would result from the interfusion of spherical micelles. The dependences of assembly morphology and assembly size on L_{PSt} are comparable to the results of Table 1.

When the molar ratio of St/PAA-DMP reached the value of 500, L_{PSt} increased to 379 and the vesicle morphologies of PAA-*b*-PSt assembly were solely observed, as shown in Figures 4B and 5C. The vesicles are different from the size (80−200 nm in diameter), wall thickness (20−50 nm), shape (regular sphere vs concave sphere), and inner structure (close vesicle vs kippah vesicle), suggesting the polydispersity of copolymer composition. Recalling the data in Table 1, we assume that the critical

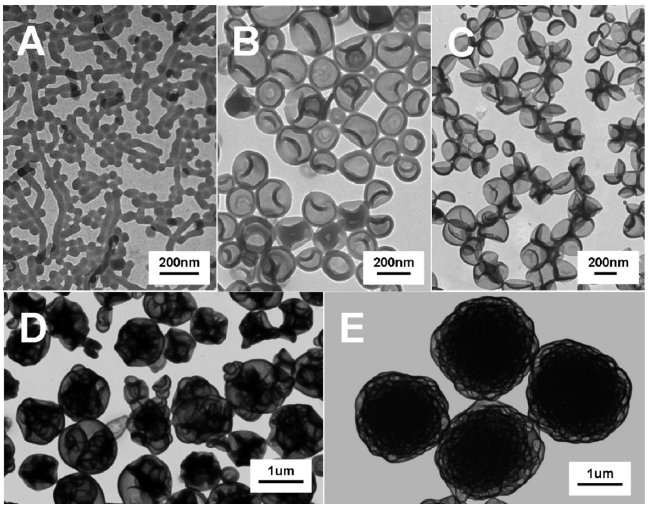

Figure 4. TEM images of PAA-*b*-PSt assemblies formed at different molar ratio. St/PAA-DMP = (A) 250, (B) 500, (C) 750, (D) 1000, and (E) 1250.

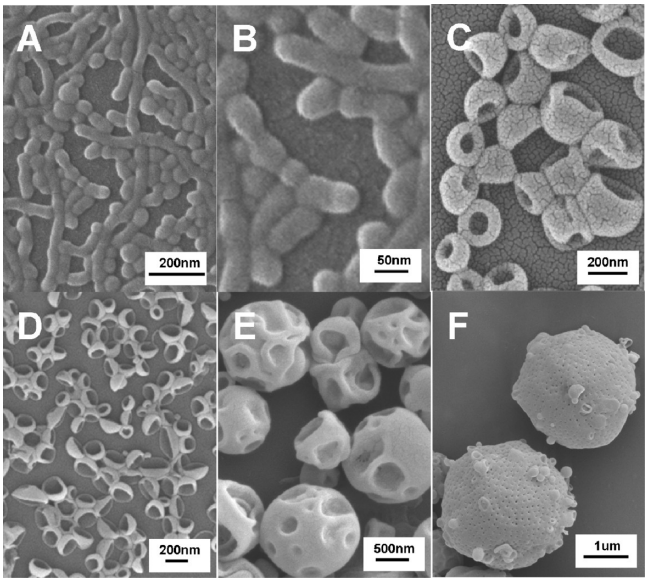

Figure 5. SEM images of PAA-*b*-PSt assemblies formed at different molar ratio. St/PAA = (A,B) 250, (C) 500, (D) 750, (E) 1000, and (F) 1250.

value of L_{PSt} for the transition of micelles to vesicles would be 379 and the reorganization of vesicles at this moment would happen through endo-uptaking mechanism.

With the further increase in St/PAA-DMP molar ratio to 750, L_{PSt} value was 537 and the vesicles were reorganized through wall-fusion mechanism, as distinguished in Figures 4C and 5D. However, the size and wall thickness of individual simple vesicles of PAA_{61}-*b*-PSt_{537} are obviously smaller than those of PAA_{61}-*b*-PSt_{379}. Similar phenomenon also appears in Figure 2. The results might be caused by the compact rearrangement of PSt block chains. At the higher molar ratio of St/PAA-DMP (1000), L_{PSt} value got to 704, and large compound vesicles were formed. These LCVs are polydispersed with a size range of 500−1000 nm. The absorption and fusion of small vesicles onto LCVs is also detected, as shown in Figures 4D and 5E.

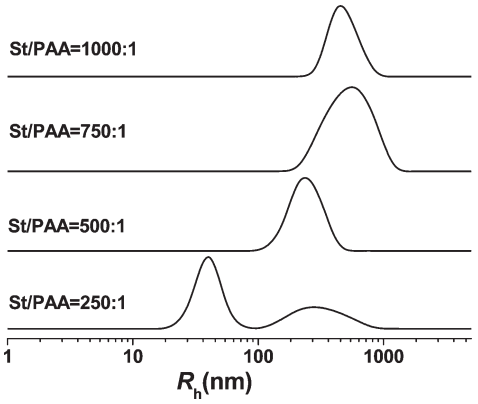

Figure 6. R_h distribution of PAA-*b*-PSt assemblies at different molar ratios of St/PAA-DMP.

Larger, more compact and uniform LCVs are observed in Figure 4E when the ratio of St/PAA-DMP increases to 1250. Surface morphology of these complicate LCVs is shown in Figure 5F. Many holes exist, and some small vesicles are adhered on the surface. These observations suggest that both the outer absorption of small vesicles onto LCVs and the inner fusion of PSt walls took place during the reorganization of vesicles.

Figure 6 shows the hydrodynamic radius distributions of the above dispersions. At St/PAA-DMP of 250, the distribution of PAA-*b*-PSt assemblies is bimodal, indicating the coexistence of the spherical and cylindrical micelles. At St/PAA-DMP of 500, PAA_{61}-*b*-PSt_{198} assemblies have R_h of 101 nm and R_g/R_h of 0.94, suggesting that they are mainly simple vesicles. With the further increase in St/PAA-DMP, the hydrodynamic radius distribution turns broader (St/PAA-DMP = 750) and then narrower (St/PAA-DMP = 1000), whereas R_h increases from 477 to 733 nm.

Influence of Methanol Amount on Assembly Morphology. The solvent property also affects the morphology transition of PAA-*b*-PSt during RAFT dispersion polymerization. Thus, RAFT dispersion polymerizations of St (1.04 g) with PAA-DMP (0.01 mmol) and AIBN (0.001 mmol) were performed in methanol (0.50, 0.75, 1.00, 1.25, 1.50, and 2.00 g) at 80 °C for 20 h. The results are summarized in Table 3, and TEM images are illustrated in Figure 7.

After a PSt-rich region such as the core of micelles and the wall of vesicles is formed, styrene monomer distributes between PSt-riched region and polymerization medium. Because the solubility parameter of St other than methanol is fairly close to that of PSt, styrene acts as a good solvent and methanol acts as a nonsolvent for PSt.

When methanol amount was as high as 1.50 or 2.00 g, only spherical micelles were produced. Higher content of methanol induces PSt chains to take more compact conformation, which makes the morphology transition difficult. The result is consistent with the previous reports, where only spherical micelles were formed because of the poor affinity of polymerization medium with PSt core-forming blocks.[44−48] Through soapless emulsion, polymerization of St with poly(methacrylic acid) macro-RAFT agent in water[66] or RAFT dispersion polymerizations of styrene at high mass ratio of ethanol to styrene (10:1),[67] Choe et al. also only obtained solid spherical particles.

As the methanol amount decreased, the final value of L_{PSt} became longer and longer, thermodynamically favorable for the morphology transition from micelles to vesicles.[2] At the same

Table 3. Characteristics of Morphologies Obtained at Different Amount of Methanol[a]

PAA-*b*-PSt	methanol (g)	con	morphology	D^b
PAA_{61}-*b*-PSt_{827}	0.50	82.7	vesicle; trepang-like; pool-inside ring; etc.	>2 μm
PAA_{61}-*b*-PSt_{771}	0.75	77.1	simple vesicle, multipool aggregates	1.4 μm
PAA_{61}-*b*-PS_{704}	1.00	70.4	simple and pregnant vesicle	287 nm
PAA_{61}-*b*-PSt_{364}	1.25	36.4	spherical micelle;	30 nm
			simple vesicle	176 nm
PAA_{61}-*b*-PSt_{332}	1.50	33.2	spherical micelle	28 nm
PAA_{61}-*b*-PSt_{276}	2.00	27.6	spherical micelle	24 nm

[a] Polymerization condition: St/PAA-DMP/AIBN 1000:10:1 (in mole); St = 1.04 g; 80 °C, 20 h. [b] Measured by TEM.

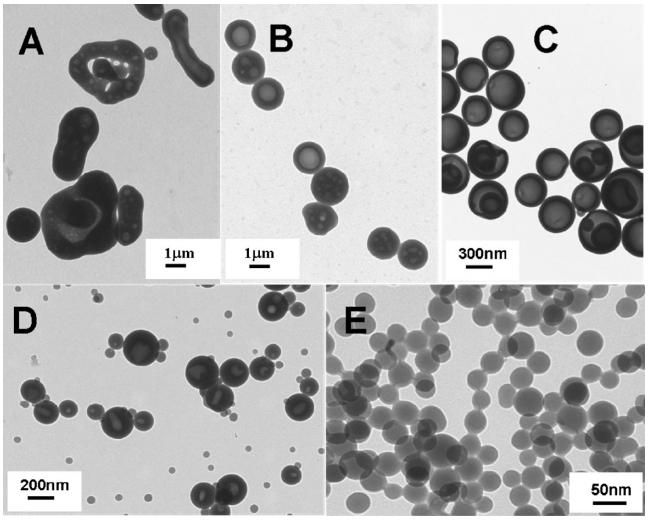

Figure 7. TEM images of PAA-*b*-PSt assemblies formed at different amounts of methanol. Methanol = (A) 0.50, (B) 0.75, (C) 1.00, (D) 1.25 g, and (E) 1.50 g.

time, the polymerization medium became better and better for the PSt block. Because PSt-riched regions were swollen to a higher and higher extent, PSt block chains would have an increasing kinetic possibility for the morphology transition. Therefore, we observed the following variation of assembly morphology with the change of methanol amount. At the methanol amount of 1.25 g, solid spherical particles coexisted with hollow spheres. The hollow spheres have much thicker "wall", quite different from the common vesicles. At the methanol amount of 1.00 g, simple vesicles and daughter-in-mother vesicles with similar wall thickness were formed. When 0.75 g methanol was introduced, simple vesicles and LCVs with multi pools were produced. Because the methanol amount was as low as 0.50 g, aggregates with much more complicated structures were formed, including trepang-like structure, irregular ring with inner pools, and doughnut with inner pools.

CONCLUSIONS

In this Article, multiform morphologies of PAA-*b*-PS were successively achieved during RAFT dispersion polymerization of styrene with trithiocarbonate-capped PAA as macro-CTA in methanol. The living/controlled behavior of RAFT dispersion polymerization led to the continuous increases in L_{PSt} throughout the polymerization and was considered to be the fundamental reason for the successive morphology transition of the obtained PAA-*b*-PSt assemblies. As for the polymerization of St (1.05 g) in methanol (1.00 g), the morphology transitions from spherical micelles, cylindrical micelles, and vesicles, to large compound vesicles were observed at the same molar ratio of styrene to PAA-CTA. With the change of St/PAA-CTA, different morphologies were also obtained at similar monomer conversion. These results demonstrate the importance of the length ratio of the core-forming to the corona-forming blocks in determining the assembly morphology of block copolymers in selective media. The critical L_{PSt} value of PAA_{61}-*b*-PSt for the transition from spherical micelle to cylindrical micelle, from cylindrical micelle to vesicle, and from vesicle to large compound vesicles was considered to be 189, 347, and 537, respectively. The coexistence of different morphologies should result from the polydispersity of PAA-*b*-PSt composition and the crossover boundaries for various morphologies. On the basis of our observation, kippah vesicles would grow into perfect vesicles by absorbing free micelles. Large compound vesicles might be produced through endo-uptaking and wall-fusion mechanisms. The increase in methanol amount in RAFT dispersion polymerization led to the different morphology assemblies, from large complicated assemblies and vesicles to spherical micelles. Although there exists other parameters affecting the in situ formation of morphology, this polymerization-induced strategy provides an efficient way to prepare different nano/microsized polymeric structures on a large scale.

ASSOCIATED CONTENT

Supporting Information. Kinetic data and analysis of living/controlled features for RAFT dispersion polymerization of St with tricarbonate-capped PAA in methanol. This material is available free of charge via the Internet at http://pubs.acs.org.

AUTHOR INFORMATION

Corresponding Author

*E-mail: wdhe@ustc.edu.cn. Tel: 86-551-3606904.

ACKNOWLEDGMENT

The financial support of NSFC (20934005), Ministry of Science and Technology of China (2007CB936401), and the HKSAR Earmarked Research Grant (403706) is greatly acknowledged. We also thank Prof. Chi Wu for the convenience of LLS measurements.

REFERENCES

(1) Zhang, L.; Eisenberg, A. *Science* **1995**, *268*, 1728–1731.
(2) Zhang, L.; Eisenberg, A. *J. Am. Chem. Soc.* **1996**, *118*, 3168–3169.
(3) Zhang, L.; Eisenberg, A. *Macromolecules* **1996**, *29*, 8805–8815.
(4) Zhang, L.; Yu, K.; Eisenberg, A. *Science* **1996**, *272*, 1777–1779.
(5) Skrabania, K.; Berlepsch, H. V.; Bttcher, C.; Laschewsky, A. *Macromolecules* **2010**, *43*, 271–281.
(6) Shah, M.; Ganesan, V. *Macromolecules* **2010**, *43*, 543–552.
(7) Chiang, W. S.; Lin, C. H.; Nandan, B.; Yeh, C. L.; Rahman, M. H.; Chen, W. C.; Chen, H. L. *Macromolecules* **2008**, *41*, 8138–8147.
(8) Hsieh, S. J.; Wang, C. C.; Chen, C. Y. *Macromolecules* **2009**, *42*, 4787–4794.
(9) Chiang, W. H.; Hsu, Y. H.; Lou, T. W.; Chern, C. S.; Chiu, C. H. *Macromolecules* **2009**, *42*, 3611–3619.
(10) Koga, T.; Tanaka, F.; Motokawa, R.; Koizumi, S.; Winnik, F. M. *Macromolecules* **2008**, *41*, 9413–9422.
(11) Antonietti, M.; Forster, S. *Adv. Mater.* **2003**, *15*, 1323–1333.
(12) Wang, D.; Wu, T.; Wan, X. J.; Wang, X. F.; Liu, S. Y. *Langmuir* **2007**, *23*, 11866–11874.
(13) Zhang, J. Y.; Xu, J.; Liu, S. Y. *J. Phys. Chem. B* **2008**, *112*, 11284–11291.
(14) Shen, L.; Du, J. Z.; Armes, S.; Liu, S. Y. *Langmuir* **2008**, *24*, 10019–10025.
(15) Cui, H. G.; Chen, Z. Y.; Zhong, S.; Wooley, K. L.; Pochan1, D. J. *Science* **2007**, *317*, 647–650.
(16) Mundargi, R. C.; Babu, V. R.; Rangaswamy, V.; Patel, P.; Aminabhavi, T. M. *J. Controlled Release* **2008**, *125*, 193–209.
(17) de Ilarduya, C. T.; Sun, Y.; Duezguenes, N. *Eur. J. Pharm. Sci.* **2010**, *4*, 159–170.
(18) Wang, Y.; Li, Z. G.; Han, Y.; Liang, L. H.; Ji, A. M. *Curr. Drug Metab.* **2010**, *11*, 182–196.
(19) Maitani, Y.; Hattori, Y. *Expert Opin. Drug Delivery* **2009**, *6*, 1065–1077.
(20) Basinska, T. *Macromol Biosci.* **2005**, *5*, 1145–1168.
(21) Nagasaki, Y. *Chem. Lett.* **2008**, *37*, 564–569.
(22) Thurmond, K. B.; Kowalewski, T.; Wooley, K. L. *J. Am. Chem. Soc.* **1996**, *118*, 7239–7240.
(23) Devereaux, C. A.; Baker, S. M. *Macromolecules* **2002**, *35*, 1921–1927.
(24) Erhardt, R.; Zhang, M.; Boker, A.; Zettl, H.; Abetz, C.; Frederik, P.; Krausch, G.; Abetz, V.; Muller, A. H. E. *J. Am. Chem. Soc.* **2003**, *125*, 3260–3267.
(25) Azzam, T.; Eisenberg, A. *Langmuir* **2010**, *26*, 10513–10523.
(26) Moore, H. D.; Saito, T.; Hickner, M. A. *J. Mater. Chem.* **2010**, *20*, 6316–6321.
(27) Jenekhe, S. A.; Chen, X. L. *Science* **1999**, *283*, 372–375.
(28) Alexandridis, P.; Olsson, U.; Lindman, B. *Macromolecules* **1995**, *28*, 7700–7710.
(29) Stepanek, M.; Kosovan, P.; Prochazka, K. *Langmuir* **2010**, *26*, 9289–9296.
(30) Breitenkamp, K.; Emrick, T. *J. Am. Chem. Soc.* **2003**, *125*, 12070–12071.
(31) Kong, W. X.; Li, B. H.; Jin, Q. H.; Ding, D. T.; Shi, A. C. *J. Am. Chem. Soc.* **2009**, *131*, 8503–8512.
(32) Ankola, D. D.; Kumar, M. N. V. R.; Chiellini, F.; Solaro, R. *Macromolecules* **2009**, *42*, 7388–7395.
(33) You, Y. Z.; Zhou, Q. H.; Manickam, D. S.; Wan, L.; Mao, G. Z.; Oupicky, D. *Macromolecules* **2007**, *40*, 8617–8624.
(34) Chen, H. W.; Zhang, Q. J.; Li, J. F.; Ding, Y. W.; Zhang, G. Z.; Wu, C. *Macromolecules* **2005**, *38*, 8045–8050.
(35) Zhang, G. Z.; Wu, C. *Adv. Polym. Sci.* **2006**, *195*, 101–76.
(36) Desbaumes, L.; Eisenberg, A. *Langmuir* **1999**, *15*, 36–38.
(37) Liu, X. Y.; Kim, J. S.; Wu, J.; Eisenberg, A. *Macromolecules* **2005**, *38*, 6749–6751.
(38) Svensson, M.; Alexandridis, P.; Linse, P. *Macromolecules* **1999**, *32*, 5435–5445.
(39) Yu, K.; Zhang, L.; Eisenberg, A. *Langmuir* **1996**, *12*, 5980–5984.
(40) Choucair, A.; Eisenberg, A. *Eur. Phys. J. E* **2003**, *10*, 37–44.
(41) Wu, C.; Niu, A. Z.; Leung, L. M.; Lam, T. S. *J. Am. Chem. Soc.* **1999**, *121*, 1954–1955.
(42) Peng, H. S.; Chen, D. Y.; Jiang, M. *Macromolecules* **2005**, *38*, 3550–3553.
(43) Chen, D. Y.; Peng, H. S.; Jiang, M. *Macromolecules* **2003**, *36*, 2576–2578.
(44) Wan, W. M.; Sun, X. L.; Pan, C. Y. *Macromolecules* **2009**, *42*, 4950–4952.
(45) Wan, W. M.; Hong, C. Y.; Pan, C. Y. *Chem. Commun.* **2009**, *39*, 5883–5885.
(46) Wan, W. M.; Sun, X. L.; Pan, C. Y. *Macromol. Rapid Commun.* **2010**, *31*, 399–404.
(47) Wan, W. M.; Pan, C. Y. *Macromolecules* **2010**, *43*, 2672–2675.
(48) Wan, W. M.; Pan, C. Y. *Macromolecules* **2007**, *40*, 8897–8905.
(49) Rieger, J.; Osterwinter, G.; Bui, C.; Stoffelbach, F.; Charleux, B. *Macromolecules* **2009**, *42*, 5518–5525.
(50) Houillot, L.; Bui, C.; Save, M.; Charleux, B.; Farcet, C.; Moire, C.; Raust, J. A.; Rodriguez, I. *Macromolecules* **2007**, *40*, 6500–6509.
(51) Ganeva, D. G.; Sprong, E.; Bruyn, H; Warr, G. G.; Such, C. H.; Hawkett, B. S. *Macromolecules* **2007**, *40*, 6181–6189.
(52) Fréal-Saison, S.; Save, M.; Bui, C.; Charleux, B.; Magnet, S. *Macromolecules* **2006**, *39*, 8632–8638.
(53) Lee, J. M.; Lee, K. S.; Min, K. J.; Choe, S. J. *Curr. Appl. Phys.* **2008**, *8*, 732–737.
(54) Wang, X. G.; Luo, Y. W.; Li, B. G.; Zhu, S. P. *Macromolecules* **2009**, *42*, 6414–6421.
(55) Song, J. S.; Winnik, M. A. *Macromolecules* **2006**, *39*, 8318–8325.
(56) Stephanie, B.; Rieger, J.; Belal, K.; Di-Cicco, A.; Beaunier, P.; Li, M. H.; Charleux, B. *Chem. Commun.* **2010**, *46*, 1950–1952.
(57) Li, Y. T.; Armes, S. P. *Angew. Chem., Int. Ed.* **2010**, *49*, 4042–4046.
(58) Sun, X. L.; He, W. D.; Li, J.; Li, L. Y.; Zhang, B. Y. *J. Polym. Sci., Polym. Chem.* **2009**, *47*, 6863–6872.
(59) Couvreur, L.; Lefay, C.; Belleney, J.; Charleux, B.; Guerret, O.; Magnet, S. *Macromolecules* **2003**, *36*, 8260–8267.
(60) Yu, Y. S.; Zhang, L. F.; Eisenberg, A. *Macromolecules* **1998**, *31*, 1144–1154.
(61) Zhang, L. F.; Eisenberg, A. *Polym. Adv. Technol.* **1998**, *9*, 677–699.
(62) Shen, H. W.; Eisenberg, A. *Macromolecules* **2000**, *33*, 2561–2572.
(63) Shen, H. W.; Zhang, L. F.; Eisenberg, A. *J. Phys. Chem. B* **1997**, *101*, 4697–4708.
(64) Yu, Y. S.; Eisenberg, A. *J. Am. Chem. Soc.* **1997**, *119*, 8383–8384.
(65) Zheng, G. H.; Pan, C. Y. *Macromolecules* **2006**, *39*, 95–102 .
(66) Wi, Y.; Lee, K.; Lee, B. H.; Choe, S. *Polymer* **2008**, *49*, 5626–5635.
(67) Shim, S. E.; Jung, H.; Lee, H.; Biswas, J.; Choe, S. *Polymer* **2003**, *44*, 5563–5572.